Applied Surface Science 459 (2018) 596–605

Contents lists available at ScienceDirect

Applied Surface Science

journal homepage: www.elsevier.com/locate/apsusc

Full Length Article

Low-temperature direct synthesis of high quality WS_2 thin films by plasma-enhanced atomic layer deposition for energy related applications

Seungmin Yeo[a,1], Dip K. Nandi[b,1], R. Rahul[b], Tae Hyun Kim[b], Bonggeun Shong[c], Yujin Jang[d], Jong-Seong Bae[d], Jeong Woo Han[e], Soo-Hyun Kim[b,*], Hyungjun Kim[a,*]

[a] School of Electrical and Electronic Engineering, Yonsei University, Seodaemun-gu, Seoul 120-749, Republic of Korea
[b] School of Materials Science and Engineering, Yeungnam University, Gyeongsan, Gyeongbuk 38541, Republic of Korea
[c] Department of Chemical Engineering, Hongik University, Mapo-gu, Seoul 04066, Republic of Korea
[d] Busan Center, Korea Basic Science Institute, 1275 Jisadong, Gangseogu, Busan 618-230, Republic of Korea
[e] Department of Chemical Engineering, Pohang University of Science and Technology (POSTECH), Pohang, Gyeongbuk 37673, Republic of Korea

ARTICLE INFO

Keywords:
Plasma-enhanced atomic layer deposition
Tungsten hexacarbonyl
Density functional theory
Tungsten disulfide
Hydrogen evolution reaction
Na-ion battery

ABSTRACT

Tungsten disulfide (WS_2) thin films are grown on several types of substrates by plasma-enhanced atomic layer deposition (PEALD) technique using tungsten hexacarbonyl [$W(CO)_6$] and H_2S plasma at a relatively low temperature of 350 °C. The method delivers polycrystalline WS_2 film with (0 0 2) preferential growth and the high quality films could be successfully grown with as low as 30 ALD cycles (corresponding to ~3 nm of thickness). Density functional theory (DFT) calculation results reveal that both adsorption of $W(CO)_6$ and removal of CO ligand would be facilitated by usage of H_2S plasma by generating the different defect sites on the basal plane. The typical self-limiting film growth (growth rate of ~0.1 nm/cycle), characteristic of ideal ALD, is clearly observed with both the precursor and reactant pulsing time. X-ray diffractometry (XRD), Raman spectroscopy, transmission electron microscopy (TEM), X-ray photoelectron spectroscopy (XPS), and Rutherford backscattering spectrometry (RBS) are performed in details to study the as-grown WS_2 film on Si/SiO_2 substrate. The analysis results confirm the formation of polycrystalline film, with high purity and well-defined stoichiometry. The as-deposited WS_2 films are then explored as an electrode in the field of energy generation as well as energy storage. The films are uniformly and conformally grown on high surface-area 3 dimensional Ni-foam that show excellent activity towards hydrogen evolution reaction (HER). Significantly low overpotential of ~280 mV is observed at a high operational current density of 100 mA cm^{-2} during HER in acid electrolyte. In addition, the as-grown films on stainless steel substrate also reveal the stable electrochemical performances in Na-ion battery as an anode with reasonably high areal capacity of ~44.5 μAh cm^{-2} at the end of 50 charge-discharge cycles.

1. Introduction

The transition metal dichalcogenides (TMDCs) have recently attracted the attention of numerous scientists, since it possess a layered structure similar to graphene that could exhibit either semiconducting or metallic properties. In layered structures of TMDCs, each layer typically has a thickness of 6–7Å, and consists of a hexagonally packed layer of metal atoms sandwiched between two layers of chalcogen atoms. The consecutive layers are further held by the weak van der Waals forces which can be easily exfoliated and yield up to a mono layer of that corresponding TMDC. Among TMDCs, W- and Mo-based (MoS_2, WS_2, WSe_2, etc.) have distinctive properties such as excellent on/off current ratio, indirect band gap to direct band gap transition, strong photoluminescence [1]. Therefore, TMDCs are expected to be a possible component in future electronic, optoelectronic and energy harvesting devices. Tungsten disulfide is particularly interesting, since the bulk WS_2 has an indirect band gap of ~1.3 eV, whereas monolayer WS_2 is a direct band gap semiconductor with a band gap of ~2.1 eV. In addition, WS_2 monolayers have been reported to exhibit an excellent on/off current ratio of 1×10^8 and carrier mobility greater than 200 $cm^2 V^{-1} S^{-1}$ [2,3]. This material, therefore, finds a lot of potential applications, such as transistors [4,5], lithium-ion batteries [6–10], solid lubricant [11–13], and chemical sensors [14–16] either in thin films or as a bulk form.

Many studies have been reported for the growth of WS_2 (Table 1), mainly using chemical vapor deposition (CVD) [4,5,17], reactive

* Corresponding authors.
E-mail addresses: soohyun@ynu.ac.kr (S.-H. Kim), hyungjun@yonsei.ac.kr (H. Kim).
[1] These authors equally contributed.

https://doi.org/10.1016/j.apsusc.2018.07.210
Received 5 July 2018; Accepted 29 July 2018
Available online 03 August 2018
0169-4332/

Table 1
Various deposition methods for WS_2 thin films.

Deposition methods	Growth temperature (°C)	Crystallinity	Composition (W:S ratio)	Ref.
CVD	500–700	N.A	N.A	[4]
	250–600	Nano crystalline	1: 1.1 to 2.0	[18]
	880–900	N.A	N.A	[17]
ALD	300	N.A	N.A	[13]
Sputtering	< 700	Polycrystalline	1:2	[18]
Solution method	100 (Dip coating) 200–1000 (annealing)	Polycrystalline	1:2	[19]
Sulfurization	500	N.A	–	[20]
	> 800	N.A	1:2	[21]

sputtering [18], solution method [19], sulfurization of W and WO_3 film [20,21]. For CVD process, it is difficult to achieve perfect stoichiometry of WS_2 and hence requires higher deposition temperature. For example, Carmalt et al. [18] reported that the WS_2 film by CVD using various W precursors such as WCl_6, $WOCl_4$ and $W(CO)_6$ at various temperatures exhibit different W to S ratio (varied from 1.3 to 2.0) depending on the precursor, deposition temperature and precursor flow conditions. On the other hand, other process such as solution method, sputtering, and sulfurization, give good stoichiometry, but, still requires a high deposition temperature or post-annealing. Orofeo et al. [21] and Rachel et al. [22] reported the synthesis of WS_2 film by sulfurization of magnetron sputtered W films, and WO_3 film at 500 and 800 °C.

Recent investigations suggest that WS_2 can also be a promising alternate to Pt for catalyzing hydrogen evolution reaction (HER) like MoS_2 in spite of the relatively few reports as compared to MoS_2 [23–27]. The literature reported overpotential values for bulk WS_2 is ~340 mV at a current density of 10 mA cm^{-2} [25], whereas, for exfoliated WS_2 nanosheets, the reported overpotential values ranges from ~310 mV to 150 mV [24–27]. Those values are generally at low current density; 10 or 25 mA cm^{-2}. At a relative higher current density of 50 mA cm^{-2} Han et al. observed an overpotential of ~320 mV on WS_2 nanosheet catalysts [28]. Recently, Shang et al. reported a current density of 100 mA cm^{-2} at ~440 mV for WS_2 nanosheet arrays catalysts on 3D high surface area carbon fiber support [29]. Most of the studies for electrocatalytic HER on WS_2 were performed on powder catalysts coated to different substrates, mainly, carbon paper or porous carbon powder. Carbon is mainly used as the substrate since, electrically conducting substrate with high surface area and porosity would be advantageous for fabricating electrode for HER. In view of this, nickel (Ni) foam is a good choice because it has very high surface area and metallic conductivity. But, Ni is highly unstable in acid condition and hence cannot be used in electrolyzer, where the metal is in direct contact with the acid electrolyte. However, recent literature reports suggest some mitigation strategy for Ni dissolution by alloying with metals such as Mo or by the coating with a thin layer of carbon [30–33]. The best way to protect the Ni from dissolution, and concurrently enhancing the HER activity, is by a conformal coating of Ni-foam with active and stable material such as WS_2. Unfortunately, all of the conventional deposition methods for WS_2 aforementioned for this purpose has limitations in this regard such as poor process controllability, limited conformality, required high process temperature, relatively complex process with post sulfurization process. Therefore, a new preparation method is needed for producing high-quality and conformal WS_2 films in a simple manner.

In these respects, atomic layer deposition (ALD) of these materials have drawn much attention because ALD uses a self-limited film growth mode by surface saturated reaction of precursors and reactants, which can provide excellent conformality, large area uniformity, and controllability of the film thickness. Unfortunately, ALD of the WS_2 process is not much explored; Song et al. reported the sulfurization of ALD grown WO_3 film [34]. This process showed systematic layer controllability and wafer level uniformity. However, needs a sulfurization step at a temperature range of 470 to 1000 °C. Few reports on ALD grown film of WS_2 without post-annealing or sulfurization can be found in the literature; for example, polycrystalline WS_2 films were deposited using WF_6 and H_2S at low-temperature range of 300–350 °C. However, this process needs the addition of reducing agents such as diethylzinc, sacrificial Si layer, and H_2 plasma [13,35,36]. Recently, Nandi et al. reported the formation of amorphous WS_2 film using $W(CO)_6$ precursor and H_2S at a low ALD temperature of 175 and 205 °C. In this process, the as-grown films are amorphous and growth rate was higher than WF_6 based process, but still as low as 0.1 Å/cycle [7].

In this study, crystalline and stoichiometric WS_2 films were grown without any post-sulfurization process using $W(CO)_6$, a novel emerging precursor for low-temperature ALD synthesis, and H_2S plasma as the reactant at a temperature of 350 °C. Density functional theory (DFT) calculation results showed that the use of H_2S plasma was crucial for a successful growth of WS_2 film by generating the different defect sites on the basal plane. The developed ALD process is used to deposit a conformal WS_2 thin film on high surface-area 3-dimensional (3D) Ni-foam for the first time to make electrode for HER in an acid electrolyte. These films were also directly grown on 2D stainless steel coin and were tested as a stable anode in sodium-ion batteries (SIBs) without any binder and conductive carbon.

2. Experiments

The WS_2 thin films were deposited on Si/SiO_2 (~ 100 nm thermally grown SiO_2 on Si wafres), stainless steel (SS) coin, and Ni-foam substrates using a showerhead-type ALD (ALD) reactor (Lucida-M100, NCD Technology) with $W(CO)_6$ and H_2S plasma as the precursor and reactant, respectively. The precursor was a white powder at room temperature with a vapor pressure of 0.8 Torr at 40 °C. The W precursor was vaporized in a bubbler at 40 °C and carried to the chamber by Ar gas at 50 standard cubic centimeters per minute (sccm). The line temperature for precursor delivery was kept at 100 °C to prevent any unintentional condensation. H_2S gas was delivered with a flow late of 50 sccm. During reactant pulsing, a radio frequency (RF) power of 100 W (W) was applied to the showerhead to ignite the corresponding plasma. After the precursor pulse and reactant pulse, a purge with 200 sccm of Ar was performed for 10 s.

Density functional theory (DFT) calculation was performed with Vienna ab initio simulation package (VASP) [37] with PBE functional [38] and projector augmented wave (PAW) method [39]. Tkatchenko-Scheffler method [40] was applied for dispersion corrections. A (4 × 4 × 1) Monkhorst-Pack k-point mesh and energy cutoff of 450 eV was used. A (4 × 4) unit cell of WS_2(0 0 2) monolayer slab was considered as substrate. Each slab was separated for more than 15 Å in the vertical direction. Using this method, the lattice constant of a monolayer WS_2 of a = 3.16 Å could be calculated close to the experimental value and previous calculations [41,42]. In addition to the pristine WS_2(0 0 2) surface, types of point defects with the highest density on related MoS_2 [43], namely, S vacancy, W vacancy, and W_{S2} antisite, were considered as adsorption sites for $W(CO)_6$. All atoms were allowed to relax until residual force becomes less than 0.02 eV/Å.

The properties of the WS_2 films were analyzed using the following techniques. The thickness of the WS_2 film was determined by atomic force microscopy (AFM) measurements after the WS_2 films were transferred to new SiO_2 substrates. The phase and crystallinity were confirmed using grazing-incidence angle (incident angle θ = 3°) X-ray diffraction (GIAXRD, PANalytical X'-pert PRO MRD with Cu- Kα radiation at 1.5 kW) analysis. The film composition and impurities were measured using Rutherford backscattering spectrometry (RBS) using He^{++} ions with incident energy of 2 MeV. X-ray photoelectron spectroscopy (XPS, Thermo Fisher Scientific Inc., K-Alpha$^+$ XPS Spectrometer in Korea Basic Science Institute at Busan, Korea) was

performed to examine the chemical bonding of the WS_2 films. Plan-view bright field transmission electron microscopy images (TEM, Tecnai F20 equipped with a 200 kV accelerating voltage and a field emission gun) were used to examine the microstructure of WS_2 films. The plan-view and cross-sectional view scanning electron microscopy (SEM, Hitachi, S-4800) images on different substrates were obtained further to show the uniform and conformal deposition of the material by this technique.

The developed ALD process is used to deposit a conformal WS_2 thin film on high surface-area 3D Ni-foam for HER in an acid electrolyte. The measurements for electrochemical HER were performed using an Ivium-n-Stat Potentiostat/Galvanostat (IVIUM Technologies, Netherlands) in a conventional three-electrode setup with Ag/AgCl (3.5 M KCl) as the reference electrode and platinum plate (1 cm^2) as a counter electrode, and 0.5 M H_2SO_4 as the electrolyte. The working electrode was WS_2 coated Ni-foam (1 cm × 1 cm × 0.14 mm, length × breadth × thickness) immersed in the electrolyte. WS_2 was deposited on Ni-foam substrate at 350 °C with 200 ALD cycles. For convenience the potential of working electrode is reported verses reversible hydrogen electrode (RHE) in this manuscript.

For further SIBs application, WS_2 thin films were directly grown on 2D stainless steel (SS) current collector (diameter 1.5 cm) using 200 ALD cycles under the self-limiting conditions as discussed later in this article. The ALD grown WS_2 film on SS was then used as an anode in SIBs under half-cell configuration against Na without any further modification. Therefore, it differs with the conventional electrode fabrication which usually contains conducting carbon and binder with the active material. Standard, 1 M $NaPF_6$ in 1:1 (by volume %) ethylene carbonate/dimethyl carbonate (EC/DMC) solution was used as electrolyte. The electrochemical studies were carried out for these coin-type cells within a potential window of 0–3 V in a standard battery tester unit (SE-18603, Famtech) at ambient room temperature.

3. Results and discussion

WS_2 films were synthesized by PEALD using $W(CO)_6$ and H_2S plasma without post sulfurization. The basic condition with 10 s pulsing of $W(CO)_6$, H_2S plasma and 10 s pulsing of Ar purging between them were set until unless stated otherwise. The ALD process can be mostly well characterized by this unique feature of the self-limiting growth of the material as discussed in the Supporting information with the associated figures (Figs. S1 and S2). Based on these experiments, the basic pulsing condition to guarantee the self-limiting growth was determined as 10 s pulsing of both $W(CO)_6$ as well as H_2S plasma with Ar purging of 10 s in between the alternate exposure of these two. A similar self-limiting growth was also reported for PEALD MoS_2 using $Mo(CO)_6$ and H_2S plasma [44]. The thickness of WS_2 films was confirmed by atomic force microscopy (AFM; Fig. S3).

Supplementary data associated with this article can be found, in the online version, at https://doi.org/10.1016/j.apsusc.2018.07.210.

DFT calculation results show that H_2S plasma treatment greatly enhances both half reactions of ALD, compared to H_2S molecular. Fig. 1 (a) summarizes calculated adsorption energy for dissociative adsorption of $W(CO)_6$ on WS_2 surface. It is reasonable to assume that plasma treatment during PEALD process would create defect sites on WS_2 substrate. Adsorption of W species on WS_2 surface during the $W(CO)_6$ pulse can be facilitated by such defects. While dissociative adsorption of $W(CO)_6$ into $*W(CO)_5$ and *CO (Fig. 1) is endothermic for pristine WS_2(0 0 2) basal plane, the same reaction becomes exothermic on all types of defects considered. Desorption of CO dissociated from $W(CO)_6$ can irreversibly deposit W to the adsorption site, and the defect sites are also less endothermic for this reaction compared to the pristine surface, making W deposition more viable. On the other hand, during the H_2S plasma pulse, incoming S-containing molecules or radicals will replace

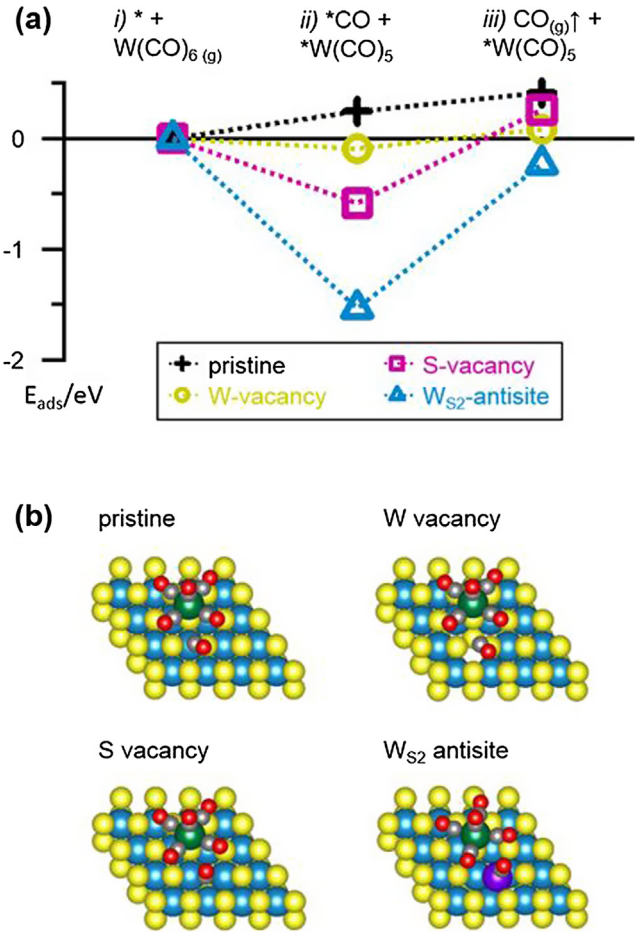

Fig. 1. (a) Calculated adsorption energy (E_{ads}, eV) for dissociative adsorption of $W(CO)_6$ on a WS_2(0 0 2) monolayer. (b) DFT-optimized geometries of $*W(CO)_5$ and *CO co-adsorbed on WS_2 monolayers (state *ii* of (a)). Gray = C, red = O, yellow = S, teal = W in WS_2 slab, green = W of $*W(CO)_5$, and purple = anti-site W. * denotes an adsorption site on the WS_2 surface.

remaining CO ligands of the surface-adsorbed W-species (Table 2). However, substitution of CO of $*W(CO)_5$ by molecular H_2S involves large endothermicity over 1 eV regardless of the substrate and thus would occur with small probability. The same ligand exchange is exothermic with SH radical, a representative reactive species that can be formed under plasma environment [45]. Therefore, deposition of S is also facilitated by RF plasma. If H atoms of SH remain after substitution of all CO, they would desorb as H_2S or H_2 from WS_2 at the deposition temperature used [46].

Fig. 2 shows grazing incidence angle (θ = 3°) XRD patterns of the WS_2 film deposited with increasing number of ALD cycles. One strong XRD peak (at 2θ = 14.378°) corresponding to the hexagonal phase of WS_2 (space group $P6_3/mmc$; JCPDS 08–0237) was clearly observed for all of these samples. The intensity of this (0 0 2) peak of hexagonal WS_2 was found to increase continuously as the ALD cycles were increased. The peak intensity became very strong for the film grown by 100 ALD cycles. This phenomenon could be easily understood by the presence of more number of the parallel planes as the film becomes thicker. Here, we assume that this PEALD grown WS_2 films would attain the properties similar to that of a bulk WS_2 in this case after 100 ALD cycles of deposition. Therefore, predominantly (0 0 2) oriented growth on Si/SiO_2 substrate could be confirmed by this XRD analysis. In this regard, we would also like to bring into notice that the earlier PEALD of WS_2 produced the crystalline film using ternary reaction cycle consisting of

Table 2
DFT-calculated reaction energy (eV) for dissociative adsorption of $W(CO)_6$ on a WS_2(0 0 2) monolayer, and subsequent substitution of CO ligand of surface-adsorbed $W(CO)_5$ with H_2S or SH. * denotes an adsorption site on the WS_2 surface.

	pristine	W vacancy	S vacancy	W_{S2} antisite
$W(CO)_{6(g)} + * \rightarrow *W(CO)_5 + *CO$	+0.25	−0.09	−0.58	−1.54
$W(CO)_{6(g)} + * \rightarrow *W(CO)_5 + CO_{(g)}$	+0.41	+0.08	+0.26	−0.23
$*W(CO)_5 + H_2S_{(g)} \rightarrow *W(CO)_4(H_2S) + CO_{(g)}$	+1.25	+1.25	+1.12	+1.23
$*W(CO)_5 + SH_{(g)} \rightarrow *W(CO)_4(SH) + CO_{(g)}$	−0.34	−0.50	−0.89	−0.75

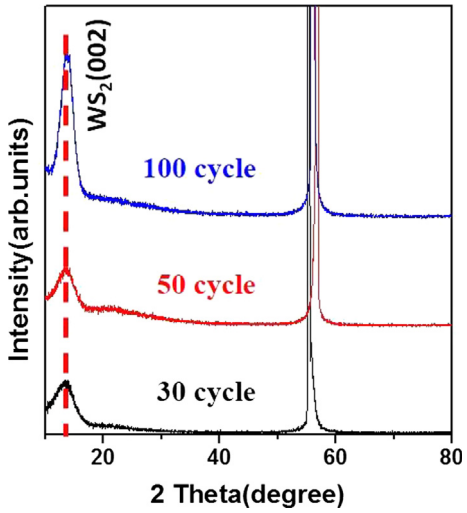

Fig. 2. Grazing-incidence angle X-ray Diffraction (GIAXRD) analysis result on ALD-WS_2 film with the number of ALD cycles.

WF_6, H_2 plasma, and H_2S molecule at a deposition temperature of 300 °C [36]. But, thermal ALD of WS_2 produced the amorphous film using same precursor $W(CO)_6$ as a source for W [7]. Therefore, it could be well inferred that the H_2S plasma as a reactant facilitates the formation of crystalline WS_2.

Once the XRD proved the crystalline growth of the PEALD-WS_2 with its most favorable and preferential direction of (0 0 2), we further carried out Raman spectroscopy to investigate the material in more details. Raman spectroscopy measurements were performed using 532 nm laser excitation. Fig. 3 (a) shows the Raman spectra of the WS_2 film with increasing number of cycles. Two prominent peaks at 360.5 cm^{-1} and 423.1 cm^{-1} were observed clearly. The peak at 360.5 cm^{-1} corresponds to a combination of the in-plane phonon mode, E^1_{2g}, and 2LA(M) peak. On the other hand, 423.1 cm^{-1} peak corresponding to the out-of-plane phonon mode can be assigned as an A_{1g} mode of Raman vibration as represented in the schematic Fig. 3 (b). The peak distance between A_{1g} to E^1_{2g} was increasing as the number of ALD cycles was increased. As the number of ALD cycles increased from 50 to 100, the peak distance between A_{1g} to E^1_{2g} shows an increase from 62.6 to 64.7 cm^{-1}. This observation is good agreement with the previously reported result for WS_2 [12,47].

Fig. 4 (a), (b), and (c) show the TEM analysis results of the representative ALD-WS_2 film deposited with the basic pulsing condition, which confirmed the phase and characterized the microstructure of the WS_2 film in details. The plan-view TEM bright-field (BF) image of the WS_2 film deposited with 30 ALD cycles on SiO_2 substrate shows polycrystalline grains with sizes ranging from 3 to 7 nm, as shown by Fig. 4 (a). The corresponding selected-area electron diffraction (SAED) pattern was matched with the hexagonal structure of WS_2, which is consistent with the XRD results as well. Fig. 4 (b) also presents a plan-view TEM high resolution (HR) image of WS_2 deposited with 30 ALD cycles with a higher magnification. A honeycomb-like structure and 6-fold coordination symmetry were observed and the fast Fourier transformation [inset in Fig. 4 (b)] which clearly showed a spot pattern in reciprocal space, indicating the formation of a single crystal with a size of ~5 nm. To extract the lattice spacing and crystal direction precisely, inverse fast Fourier transformation was performed by applying a mask to the inset figure in Fig. 4 (b) using the Gatan Digital Micrograph software package, leading to a constructed HR image [Fig. 4 (c)]. From the constructed HR image, the lattice spacing in each direction was determined from the intensity profile [Fig. 4 (d)] and was found to be 0.27 nm which corresponds to the (1 0 0) planes of hexagonal WS_2.

Fig. 5 (a) shows the RBS spectra of the WS_2 film (~30 nm-thick) deposited with the basic pulsing condition on the SiO_2 (100 nm in thickness) coated Si wafers (~ 500 μm in thickness). When the incident energy of He^{++} is 2 MeV as shown in Fig. 5 (a), a backscattered peak

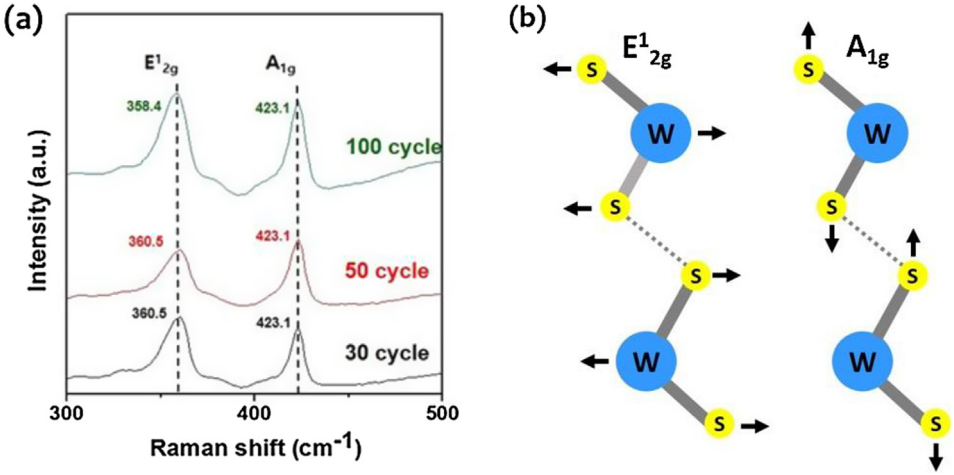

Fig. 3. (a) The Raman-spectroscopy results of the ALD WS_2 films on the SiO_2 substrate as a function of a number of cycles and (b) the schematic figure of the two Raman vibration modes.

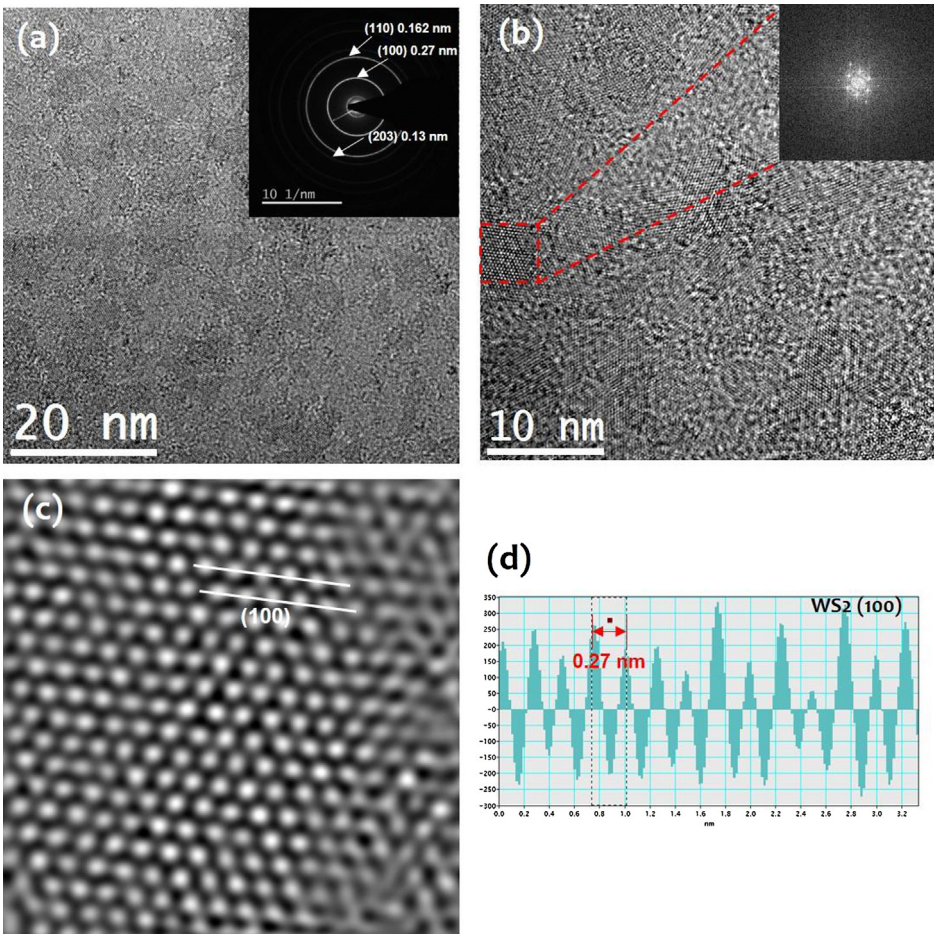

Fig. 4. Plan-view TEM image of ALD-WS_2 films; (a) bright-field image of ALD-WS_2 film deposited on SiO_2 (the inset shows the SAED pattern of the film), (b) high resolution (HR) image, (c) the constructed HR image from the Fourier transformation of the real HR image, and (d) the line profile showing the layer spacing in (c).

from W in the deposited film is clearly shown in the channel number from ~880 and ~960. The backscattered peak shown at the channel number of ~620 was from S in the film. Backscattered peaks from Si consist of 2 different positions. The first peak is at the channel number of ~560, which is the backscattered one due to the collision of He^{++} with Si in the thermally grown SiO_2. The second peak is from Si wafer itself which was observed at the channel number of ~530 with the highest yield. The backscattered peak shown at the channel number of ~350 was from O in the SiO_2. By using the RUMP simulation for RBS analysis, the ratio of W and S (W/S) was determined as ~2 ($W_{1.03}$ S_2) which indicates the stoichiometric deposition of WS_2 films beyond doubt.

XPS was performed further to confirm the constituent element, chemical composition and the oxidation state of the W in the WS_2 film by determining the corresponding binding energies of W and S electrons (Fig. 5 (b) and (c)). The XPS data were obtained after sputtering an approximately 4-nm-thick film at the surface to exclude the C and O contamination and to characterize the bonding status of the film itself. The XPS data was calibrated with the adventitious C 1 s peak (284.5 eV) detected on the film surface. Fig. 5 (b) shows the spectrum of W *4f* photoelectrons. The doublet of W*4f* orbital electrons at the binding energies at ca. 35 and 33 eV can be assigned respectively to the $4f_{5/2}$ and $4f_{7/2}$ electronic states of W in W-S bond. These binding energies of W*4f* orbital electrons in the as-grown film also indicate the W^{+4} oxidation state of W confirming the chemical composition as WS_2. The XPS spectrum corresponding to the *2p* binding energies of S is shown in Fig. 5 (c). The peaks at a binding energy of ca. 162.8 eV and 164 eV, as obtained after the XPS peak fitting, are attributed to the $S2p_{3/2}$ and $S2p_{1/2}$ electronic states, respectively for the divalent sulfide ions (S^{2-}) present in the film. Thus, all the analysis results clearly showed that polycrystalline, pure, and stoichiometric WS_2 films and nano-sheets were successfully and directly grown using a present scheme of PEALD using $W(CO)_6$ precursor and H_2S plasma at a relatively low temperature of 350 °C without any post process.

The electrocatalytic hydrogen evolution activity of PEALD-WS_2/3D Ni-foam catalysts is examined for the first time in 0.5 M H_2SO_4. The WS_2 film is directly grown on Ni-foam using 200 ALD cycles and is used as an active electrode in HER without any further treatment. Fig. 6 shows the plane-view SEM images of WS_2 coated 3D Ni-foam electrode and corresponding images of the bare Ni-foam at similar magnifications; clearly exhibiting uniform and conformal coating of WS_2 on Ni-foam surface. While the unique potential of ALD to coat a thin film on any complex substrate like Ni-foam is truly clear from Fig. 6 (a) and (b), the presence of the material becomes obvious by comparing the SEM images at relatively higher magnifications. Moreover, WS_2 nano-flakes formation on Ni-foam surface without affecting the porous nature of Ni-foam is evident from these images (Fig. 6 a, c, and e). Such nano-flake like structure might be due to the highly preferential growth at (0 0 2) direction as revealed by the XRD and also could be influenced to some extent by the Ni-foam substrate. Similar 3D growth during ALD of some other materials like MoS_2 and V_2O_5 with increasing ALD cycles are also reported in the literature [48,49]. Interestingly, the 3D nano-morphology of this present material on porous Ni-foam is an added advantage of the composite towards HER application due to its extremely high exposed surface for catalytic reaction. The energy dispersive X-ray spectroscopy (EDS) of this composite and the individual elemental

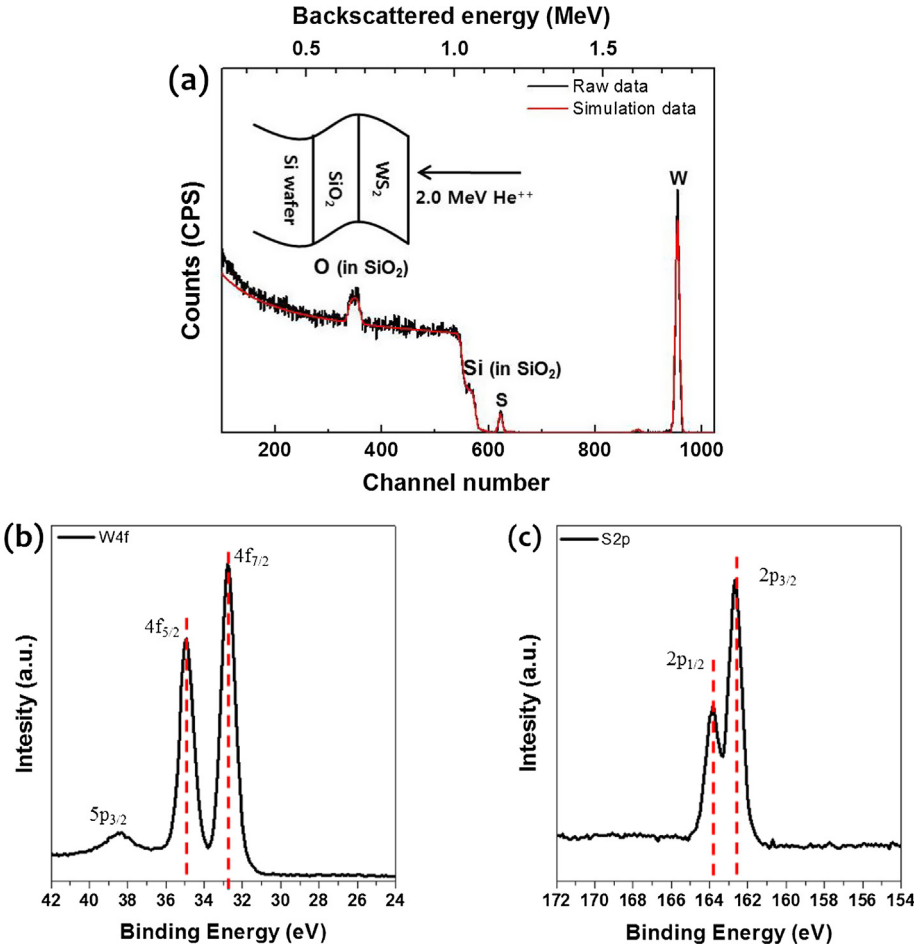

Fig. 5. (a) RBS spectra of the ALD-WS_2 film deposited of substrate temperature was 350 °C on SiO_2 (100 nm in thickness) covered Si wafer with incident H_2^{++} energies was 2 MeV. (b)W 4f, and (c) S 2p XPS spectra of the ALD-WS_2 films.

mapping of W, S and Ni further reveals the successful preparation of this material for HER application (please see Fig. S4).

Fig. 7 (a) shows the linear sweep voltammogram (LSV) of WS_2/Ni-foam catalysts in 0.5 M H_2SO_4 electrolyte, recorded at a scan rate of 5 mV s^{-1}. For comparison, the voltammograms of standard Pt-wire (1 cm^2) and bare Ni-foam support are also included in the figure. The onset for HER on Ni-foam is at ~ −0.24 V; indicating reasonable hydrogen evolution activity of nickel. The overpotential observed at a current density of 100 mA cm^{-2} (geometric) for platinum wire electrode is ~90 mV, and that for Ni-foam is ~360 mV, whereas, the WS_2 has overpotential of ~280 mV to achieve a current density of 100 mA cm^{-2}. In the literature, WS_2 has been reported to exhibit similar overpotential (200–300 mV) at an operating current density of 25 mA cm^{-2}. The advantage of using highly conducting Ni-foam as support for WS_2 is further evident form the voltammogram shown in Fig. 7 (b) that reflects the current densities for WS_2/Ni-foam and bare Ni-foam up to a potential window of -0.4 V vs. RHE; significantly high current densities are obtained for this composite compared to the bare substrate at lower operational potentials. In the literature, WS_2 nanosheets arrays on high surface area carbon fiber shows an overpotential of ~440 mV at an operational current density of 100 mA cm^{-2}, and when compared to that the ~280 mV is a significant enhancement. To further evaluate the activity of WS_2 and Ni-foam catalysts, Tafel plots are derived from the voltmmetric data and are shown in Fig. 7 (c). The linear portion of the plot is fitted with Tafel equation to obtain kinetic and mechanistic insight of the reaction on WS_2 surface. The Tafel slope of ~27 mV per decade observed with platinum is matching with the literature value of ~30 mV dec^{-1}, which implies that the reaction between surface adsorbed hydrogen is the rate-determining step (Tafel step) in platinum. The Tafel slope observed for bare Ni-foam is ~152 mV dec^{-1}, which is closer to the theoretical Tafel slope of Volmer step (~120 mV dec^{-1}). This implies that the formation of adsorbed hydrogen on the surface of the catalyst is the rate-limiting step in HER on nickel. The slightly higher value observed may be due to the parallel surface oxide reduction taking place during HER. The Tafel slope observed for WS_2/Ni-foam is ~63 mV dec^{-1}, a value that is closer to the ~40 mV dec^{-1} observed in case of Volmer-Heyrovsky step. Earlier reports on WS_2 also suggests the Volmer-Heyrovsky as the rate-limiting step for HER [24], the slight deviation from the theoretical 40 mV dec^{-1} may be due to the contribution from other induvial steps in HER or due to the surface oxidation/reduction reaction happening parallel to HER. The charge transfer resistance (R_{ct}), which can be derived from the semicircle in the low frequency zone of the Nyquist plots (Fig. 7d) is a measure of the rate of the reaction. A lower value for R_{ct} implies a better active catalyst. The R_{ct} (the diameter of the semicircle shown in Fig. 7d) observed for Ni-foam at an overpotential 200 mV is approximately 4.82 Ω, and at 300 mV, the R_{ct} value decreases to ~2.135 Ω. This is due to the increased HER kinetics at higher overpotential. In case of WS_2/Ni-foam the R_{ct} values obtained at overpotential of 200 mV (~3.4 Ω) and 300 mV (~1.33 Ω) are much lower than that observed on bare Ni-foam. This clearly reflects the fast electron transfer and favorable HER kinetics at the WS_2 surface.

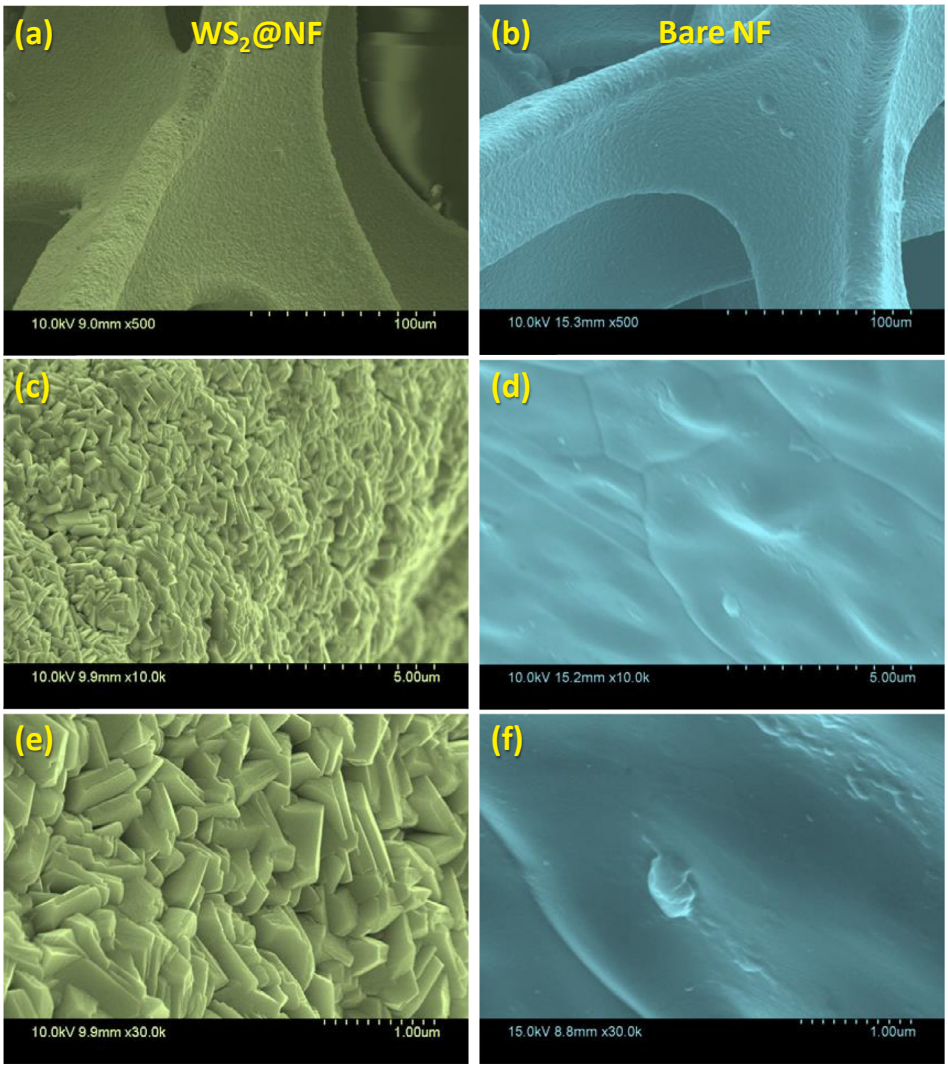

Fig. 6. Plan-view SEM image (a, c, and e) of WS_2 films grown on Ni-foam by 200 ALD cycles for HER application, and (b,d,f) bare Ni-foam at three different magnifications revealing the highly uniform and conformal coating of the material on 3D porous substrate by this technique.

In the last section of this article, we elucidate a preliminary study showcasing the potential of these directly grown PEALD-WS_2 thin films on SS substrate for a stable anode in sodium-ion batteries (SIBs). ALD was never adopted as a deposition tool to fabricate WS_2 which can be directly grown and used as an anode by for SIBs. Thus, this attempt would provide a room to explore the electrochemical reactions between pristine WS_2 and Na-ions in a better way in absence of any conducting carbon and binder. The SIBs performance of ALD grown WS_2 is evaluated on a ~21 nm WS_2 film was grown on SS substrate using 200 ALD cycles (please see the cross-sectional view SEM images in Fig. S4). Here, we also confirm the growth rate to be approximately similar to that on Si/SiO_2 substrates as studied earlier.

Fig. 8 (a) depicts the schematic of the ALD grown WS_2 as an anode under half-cell configuration with the Na-ion movement during charge-discharge process. The cyclic voltammetry (CV) of the WS_2 anode within a potential window of 0–3.0 V with a scan rate of 0.2 mV/s is shown in the Fig. 8 (b). The cathodic sweep (discharge) in the first cycle of the CV shows the prominent multi-step intercalation of Na-ion into WS_2 at 1.2 and 0.87 V, respectively. Such multi-step Na-intercalation mechanism is not a very uncommon phenomenon for TMDCs including WS_2 as well [10]. The conversion reaction followed by the insertion of Na-ion is confirmed by another prominent peak at around ~0.6 V. On the other hand, the first anodic sweep (charge cycle) revealed two distinct peaks at ~1.4 and ~1.9 V which can be ascribed to the reversible conversion and deintercalation of Na from the electrode. The reversible electrochemistry between Na-ion and WS_2 can thus be realized through the following two reactions:

$$WS_2 + x\mathrm{Na}^+ + xe^- \leftrightarrow \mathrm{Na}_x\mathrm{WS}_2 \quad (1)$$

$$4\mathrm{Na} + \mathrm{WS}_2 \leftrightarrow 2\mathrm{Na}_2\mathrm{S} + \mathrm{W} \quad (2)$$

Apart from these prominent intercalation and conversion reaction peaks, another very small peak at around ~0.34 V was also observed during the first discharge cycle which could be ascribed to the formation of solid electrolyte interface (SEI). In addition, the reversible SEI formation and deformation is clear from 2nd cycle onwards at the potential of 0.35 and 0.39 V during the discharge and charge cycle respectively. Such reversible SEI formation and dissolving also contributes to the capacity for this WS_2 anode [8] and therefore should be considered as an added advantage to this anode material. Fig. 8 (c) shows few charge-discharge profiles of this WS_2 anode. The two distinct plateaus above ~1.0 V and at around ~0.5 V in the discharge profiles

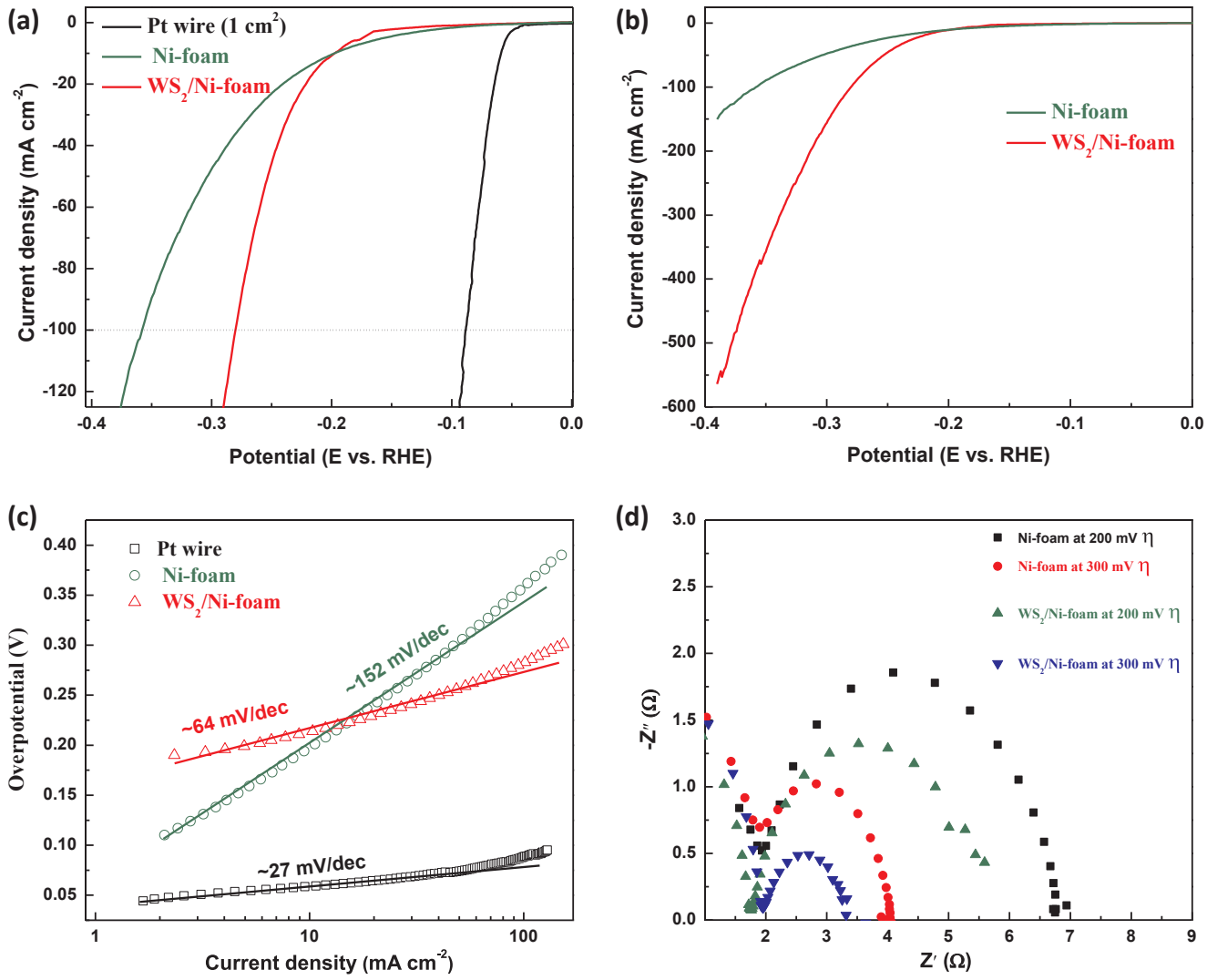

Fig. 7. (a) Linear sweep voltammogram (iR corrected) of the WS_2/Ni-foam, bare Ni-foam and Pt wire electrode in 0.5 M H_2SO_4 electrolyte at scan rate of 5 mV s^{-1} (b) LSV showing extremely high current densities of WS_2/Ni-foam during HER in a potential window of 0 to −0.4 V (c) corresponding Tafel plot derived from (b) and (d) Nyquist plots of WS_2/Ni-foam, bare Ni-foam and Pt wire electrode at 200 mV and 300 mV overpotential of HER.

reflect the intercalation and conversion of Na-ion in the WS_2 anode. On the other hand, a broad and continuous plateau between 1 and 2 V during the charging represents the multistep desodiation of the anode. Thus, these charge-discharge profiles are completely in-line with the CV measurements as discussed above. The cyclic stability and their corresponding Coulombic efficiency (CE) of this ALD grown WS_2 anode are shown in Fig. 8 (d). The resonably high areal capacity of ca. 61.5 and 44.5 μAh/cm^2 was obtained at the end of the 1st and 50th discharge cycle, respectively. Slow but continuous capacity fading for this anode was observed as revealed by this cyclic stability test. The reason for such capacity fading is the absence of the conducting carbon in the anode and therefore the resistivity of the pristine WS_2 leads to decrease in capacity upon cycling. However, reasonable capacity retention of around 72.5% was observed after 50 charge-discharge cycles for this pure PEALD-WS_2 anode. Nevertheless, the reversible capacity and its retention could be further enhanced by depositing such a thin film on a 3-dimensional conducting matrix like multi-wall carbon nanotubes (MWCNTs) [50]. Excellent CE over 98% throughout the cycling shows the easy and efficient sodiation and desodiation in this ALD grown layered WS_2 anode. Further studies related to this ALD-WS_2 anode are being carried out as a scope of the future work.

4. Summary and conclusions

Tungsten disulfide (WS_2) thin films were directly grown by PEALD using tungsten hexacarbonyl [$W(CO)_6$] and H_2S plasma at a relatively low temperature of 350 °C without any post sulfurization process. Based on systematic *ex-situ* analyses including XRD, Raman, TEM, XPS, and RBS, a very stoichiometric with the negligible incorporation of C and O impurities and poly-crystalline WS_2 with preferential (0 0 2) directional growth was evident for the as-grown films. Self-limiting film growth with the growth rate of ~0.1 nm/cycle, was observed with both the precursor and reactant pulsing time. Due to the self-limiting growth and growth rate linearity of the process, WS_2 nano-sheets could be fabricated by controlling the number of ALD reaction cycles. DFT calculation results showed that both adsorption of $W(CO)_6$ and removal of CO ligand would be facilitated by usage of H_2S plasma. The conformal WS_2 grown on 3D Ni-foam is tested as an electrode for hydrogen evolution reaction (HER), a lower overpotential of ~280 mV is observed at a high operational current density of 100 mA cm^{-2}. The high activity of WS_2 grown on 3D Ni-foam is due to the optimal thickness of the conformally grown ALD film, high surface area and good electrical conductivity of 3D Ni-foam substrate. The potential of ALD-WS_2 as a stable anode for

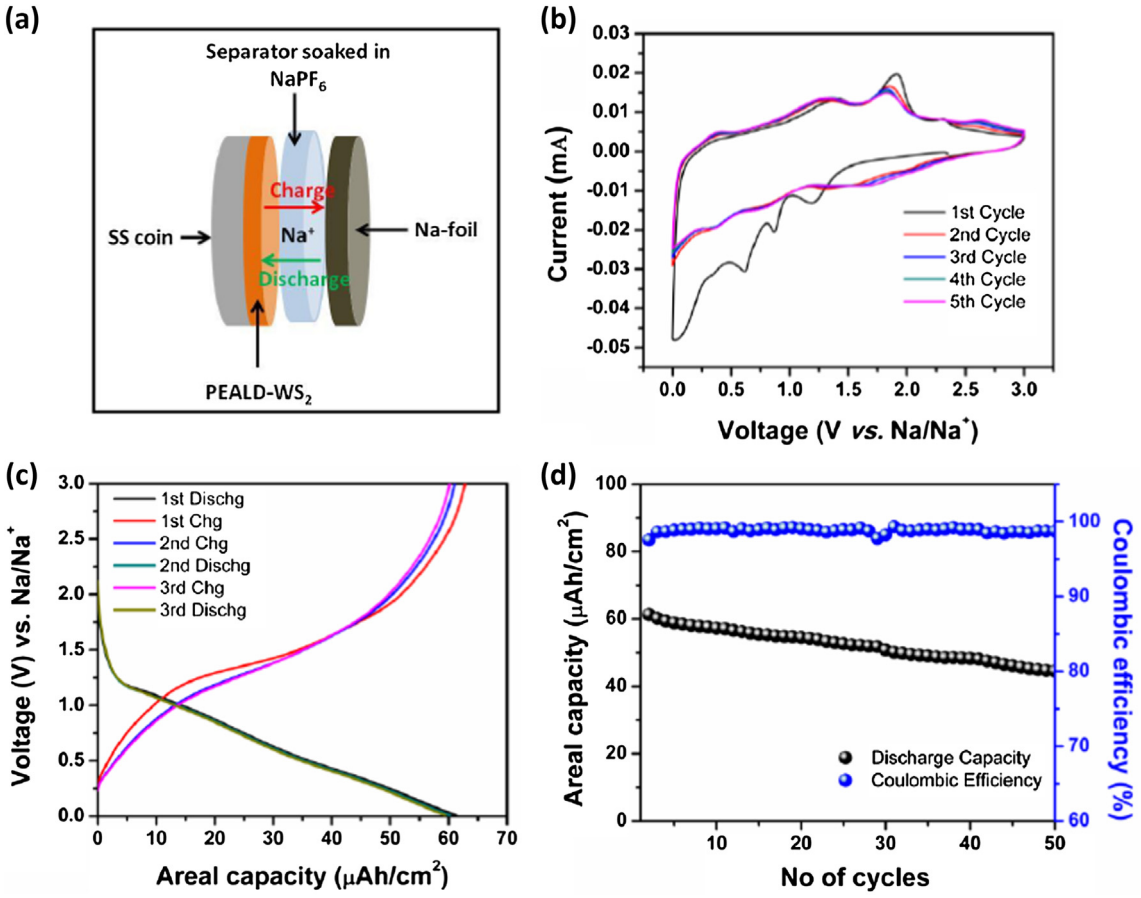

Fig. 8. (a) Schematic of the ALD grown WS_2 as an anode under half-cell configuration in Na-ion battery, (b) cyclic voltammogram of the WS_2 against Na/Na^+ in a voltage range of 0–3 V at scan rate of 0.2 mV s^{-1} (c) charge-discharge profiles for first three cycles and (d) cycling performance of WS_2 as an anode in Na-ion battery.

SIBs without any conducting carbon and binder were also evaluated. Cyclic stability test showed considerable areal capacity of ca. 44.5 μAh/cm^2 at the end of the 50th discharge cycle with excellent Coulombic efficiency over 98% throughout the cycling. We believe that this work will facilitate further to explore ALD as a direct and efficient electrode preparation technique for HER and SIBs.

5. Notes

The authors declare no competing financial interests.

Acknowledgments

This work was supported by Mid-career Researcher Program through NRF grant funded by the MEST (2015R1A2A2A04004945), Korea Basic Science Institute under the R&D program (Project No. D38700) supervised by the Ministry of Science and ICT, Republic of Korea, a grant from the Advanced Technology Center (ATC) Program (10077265, Commercialization technology development of solid transition metal chloride precursor for semiconductor thin film) funded by the Ministry of Trade, Industry & Energy of the Republic of Korea, and the MOTIE (Ministry of Trade, Industry & Energy (#10080651) and KSRC (Korea Semiconductor Research Consortium) support program for the development of the future semiconductor device. The precursor used in this study was provided by UP Chemical Co. Ltd., Korea.

References

[1] Q.H. Wang, K.K. Zadeh, A. Kis, J.N. Coleman, M.S. Strano, Electronics and optoelectronics of two-dimensional transition metal dichalcogenides, Nature Nanotech. 7 (2012) 699–712.
[2] M. Trhipuranthaka, R.V. Kashid, C.S. Rout, D.J. Late, Temperature dependent Raman spectroscopy of chemically derived few layer MoS_2 and WS_2 nanosheets, Appl. Phys. Lett. 104 (2014) 018911.
[3] M.W. Lqbal, M.Z. Lqbal, M.F. Khan, M.A. Shehzad, Y. Seo, J.H. Park, C. Hwang, J. Eom, High-mobility and air-stable single-layer WS_2 field-effect transistors sandwiched between chemical vapor deposition-grown hexagonal BN films, Scientific Reports. 5 (2015) 10699–10707.
[4] A.M. Hussain, G.A.T. Sevilla, K.R. Rader, M.M. Hussain, Chemical vapor deposition based tungsten disulfide (WS_2) thin film transistor, IEEE Saudi Int. Commun. Photon. Conf. (2013).
[5] Y. Gong, V. Carozo, H. Li, M. Terrones, T.N. Jackson, High flex cycle testing of CVD monolayer WS_2 TFTs on thin flexible polyimide, 2D Mater. 3 (2016) 021008–021013.
[6] L. Zhou, S. Yan, L. Pan, X. Wang, Y. Wang, Y. Shi, A scalable sulfuration of WS_2 to improve cyclability and capability of lithium-ion batteries, Nano Res. 9 (2016) 857–865.
[7] D.K. Nandi, U.K. Sen, A. Dhara, S. Mitra, S.K. Sarkar, Intercalation based tungsten disulfide (WS_2) Li-ion battery anode grown by atomic layer deposition, RSC Adv. 6 (2016) 38024–38032.
[8] X. Wang, J. Huang, J. Li, L. Cao, W. Hao, Z. Xu, (002)-oriented WS_2 with high crystalline with enhanced capacity as anode material for sodium ion batteries, J. Alloys. Compd. 696 (2017) 22–27.
[9] D. Su, S. Dou, G. Wang, WS_2@graphene nanocomposites as anode materials for Na-ion batteries with enhanced electrochemical performances, Chem. Commun. 50 (2014) 4192–4195.
[10] Y. Liu, N. Zhang, H. Kang, M. Shang, L. Jiao, J. Chen, WS_2 nanowires as a high-performance anode for sodium-ion batteries, Chem. Eur. J. 21 (2015) 11878–11884.
[11] C. Drummond, N. Alcantar, J. Israelachvili, R. Tenne, Y. Golan, Microtribology and

friction-induced material transfer in WS_2 nanoparticle additives, Adv. Funct. Mat. 11 (2001) 348–354.
[12] L. Rapoport, N. Fleischer, R. Tenne, Fullerene-like WS_2 nanoparticles: superior lubricants for harsh conditions, Adv. Mater. 7 (2003) 651–655.
[13] T.W. Scharf, S.V. Prasad, T.M. Mayer, R.S. Goeke, M.T. Dugger, Atomic layer deposition of tungsten disulfide solid lubricants thin films, J. Mater. Res. 19 (2004) 3443–3446.
[14] D.J. Late, R.V. Kanawade, P.K. Kannan, C.S. Rout, Atomically thin WS_2 nanosheets based gas sensor, Sensor Lett. 14 (2016) 1249–1254.
[15] M. O'Brien, K. Lee, R. Morrish, N.C. Berner, N. McEvoy, C.A. Wolden, G.S. Duesbegr, Plasma assisted synthesis of WS_2 for gas sensing applications, Chem. Phys. Lett. 615 (2014) 6–10.
[16] K.Y. Ko, J. Song, Y. Kim, T. Choi, S. Shin, C.W. Lee, K. Lee, J. Koo, H. Lee, J. Kim, T. Lee, J. Park, H. Kim, Improvement of gas-sensing performance of large-area tungsten disulfide nanosheets by surface functionalization, ACS Nano 10 (2016) 9287–9296.
[17] Y. Zhang, Y. Zhang, Q. Ji, J. Ju, H. Yuan, J. Shi, T. Gao, D. Ma, M. Liu, Y. Chen, X. Song, H.Y. Hwang, Y. Cui, Z. Liu, Controlled growth of high-quality monolayer WS_2 layers on sapphire and imaging its grain boundary, ACS Nano 7 (2013) 8963–8971.
[18] C.J. Carmalt, I.P. Parkin, E.S. Peters, Atmospheric pressure chemical vapour deposition of WS_2 fin films on glass, Polyhedron 22 (2003) 1499–1505.
[19] S. Brunken, R. Mientus, K. Ellmer, Metal-sulfide assised rapid crystallization of highly (001)-textured tungsten disulphide (WS_2) films on metallic back contacts, Phys. Status Solidi A 209 (2012) 317–322.
[20] T.Y. Chen, Y.H. Chang, C.L. Hsu, K.H. Wei, C.Y. Chiang, L.J. Li, Comparative study on MoS_2 and WS_2 for electrocatalytic water splitting, Int. J. Hydrogen Energy 38 (2013) 12302–12309.
[21] C.M. Orofeo, S. Suzuki, Y. Sekine, H. Hibino, Scalable synthesis of layer-controlled WS_2 and MoS_2 sheets by sulfurization of thin metal films, Appl. Phys. Lett. 105 (2014) 083112.
[22] R. Morrish, T. Haak, C.A. Wolde, Low-temperature synthesis of n-type WS_2 thin films via H_2S plasma sulfurization of WO_3, Chem. Mater. 26 (2014) 3986–3992.
[23] Y. Wen, Y. Xia, S. Zhang, Tungsten disulphide nanorattle: a new type of high performance eletrocatalyst for hydrogen evolution reaction, J. Power Sources. 307 (2016) 593–598.
[24] L. Cheng, W. Huang, Q. Gong, C. Liu, Z. Liu, Y. Li, H. Dai, Ultrathin WS_2 nanoflakes as a high-performance electrocatalyst for the hydrogen evolution reaction, Angew. Chem. 53 (2014) 7860–7863.
[25] M.A. Lukowski, A.S. Daniel, C.R. English, F. Meng, A. Forticaux, R.J. Hamers, S. Jin, Highly active hydrogen evolution catalysis from metallic WS_2 nanosheets, Energy Environ. Sci. 7 (2014) 2608–2613.
[26] J. Yang, D. Voiry, S.J. Ahn, D. Kang, A.Y. Kim, M. Chhowalla, H.S. Shin, Two-dimensional hybrid nanosheets of tungsten disulfide and reduced graphene oxide as catalysts for enhanced hydrogen evolution, Angew. Chem. 125 (2013) 13996–13999.
[27] Z. Wu, B. Fang, A. Bonakdarpour, A. Sun, D.P. Wilkinson, D. Wang, WS2 nanosheets as a highly efficient electrocatalyst for hydrogen evolution reaction, Appl. Catal. B: Environ. 125 (2012) 59–66.
[28] G.-Q. Han, Y.-R. Liu, W.-H. Hu, B. Dong, X. Li, Y.-M. Chai, Y.-Q. Liu, C.-G. Liu, WS_2 nanosheets based on liquid exfoliation as effective electrocatalysts for hydrogen evolution reaction, Mater. Chem. & Phys. 167 (2015) 271–277.
[29] X. Shang, K.-L. Yan, Z.-Z. Liu, S.-S. Lu, B. Dong, J.-Q. Chi, X. Li, Y.-R. Liu, Y.-M. Chai, C.-G. Liu, Oxidized carbon fiber supported vertical WS_2 nanosheets arrays as efficient 3D nanostructure electrocatalysts for hydrogen evolution reaction, Appl. Surf. Sci. 402 (2017) 120–128.
[30] Y. Zhang, Y. Wang, S. Jia, H. Xu, J. Zang, J. Lu, A hybrid of NiMo-Mo_2C/C as non-noble metal electrocatalyst for hydrogen evolution reaction in an acidic solution, Electrochem. Acta. 22 (2016) 747–754.
[31] J.R. Mckone, B.F. Sadtler, C.A. Werlang, N.S. Lewis, H.B. Gray, Ni-Mo nanopowders for efficient electrochemical hydrogen evolution, ACS Catal. 3 (2013) 166–169.
[32] W.-F. Chen, K. Sasaki, C. Ma, A.I. Frenkel, N. Marinkovic, J.T. Muckerman, Y. Zhu, R.R. Adzic, Hydrogen-evolution catalysts based on non-nobel metal nickel-molybdenum nitride nanosheets, Angew. Chem. 51 (2012) 6131–6135.
[33] W. Zhou, Y. Zhou, L. Yang, J. Huang, Y. Ke, K. Zhou, L. Li, S. Chen, N-doped carbon-coated cobalt nanorod arrays supported on a titanium mesh as highly active electrocatalysts for the hydrogen evolution reaction, J. Mater. Chem. A. 3 (2015) 1915–1919.
[34] J. Song, J. Park, W. Lee, T. Choi, H. Jung, C.W. Lee, S.-H. Hwang, J.M. Myoung, J.-H. Jung, S.-H. Kim, C.L-. Matras, H. Kim, Layer-controlled, wager-scale and conformal synthesis of tungsten disulfide nanosheets using atomic layer deposition, ACS Nano 7 (2013) 11333–11340.
[35] T.W. Scharf, S.V. Prasad, M.T. Dugger, P.G. Kotula, R.S. Goeke, R.K. Grubbs, Growth, structure, and tribological behavior of atomic layer-deposited tungsten disulphide solid lubricant coating with applications to MEMS, Acta Mater. 54 (2006) 4731–4743.
[36] B. Groven, M. Heyne, A.N. Metha, H. Bender, T. Nuytten, J. Meersschaut, T. Conard, P. Verdonck, S.V. Elshocht, W. Vandervorst, S.D. Gendt, M. Heyns, I. Radu, M. Caymax, A. Delabie, Plasma-enhanced atomic layer deposition of two-dimensional WS_2 from WF_6, H_2 plasma, and H_2S, Chem. Mater. 29 (2017) 2927–2938.
[37] G. Kresse, J. Furthmüller, Efficient iterative schemes for ab initio total-energy calculations using a plane-wave basis set, Phys. Rev. B. 54 (1996) 11169–11186.
[38] J.P. Perdew, K. Burke, M. Ernzerhof, Generalized gradient approximation made simple, Phys. Rev. Lett. 77 (1996) 3865–3868.
[39] P.E. Blöchl, Projector augmented-wave method, Phys. Rev. B. 50 (1994) 17953–17979.
[40] A. Tkatchenko, M. Scheffler, Accurate molecular Van Der Waals interactions from ground-state electron density and free-atom reference data, Phys. Rev. Lett. 102 (2009) 073005.
[41] W.J. Schutte, J.L. De Boer, F. Jellinek, Crystal structures of tungsten disulfide and diselenide, J. Sol. Stat. Chem. 70 (1987) 207–209.
[42] F. Zhang, W. Li, Y. Ma, Y. Tang, X. Dai, Tuning the Schottky contacts at the graphene/WS_2 interface by electric field, RSC Adv. 7 (2017) 29350–29356.
[43] J. Hong, Z. Hu, M. Probert, K. Li, D. Lv, X. Yang, L. Gu, N. Mao, Q. Feng, L. Xie, J. Zhang, D. Wu, Z. Zhang, C. Jin, W. Ji, X. Zhang, J. Yuan, Z. Zhang, Exploring atomic defects in molybdenum disulphide monolayers, Nat. Commun. 6 (2015) 6293–6300.
[44] Y. Jang, S. Yeo, H.-B.-R. Lee, H. Kim, S.-H. Kim, Wafer-scale, conformal and direct growth of MoS_2 thin films by atomic layer deposition, Appl. Surf. Sci. 365 (2016) 160–165.
[45] K. Gustol, T. Nunnally, A. Rabinovich, A. Fridman, A. Starikovskiy, A. Gustol, A. Kemoun, Plasma assisted dissociation of hydrogen sulfide, Int. J. Hydrogen Energy 37 (2012) 1335–1347.
[46] M. Breysse, E. Furimsky, S. Kasztelan, M. Lacroix, G. Perot, Hydrogen activation by transition metal sulfides, Catalysis Rev. 44 (2002) 651–735.
[47] J. Song, G.H. Ryu, S. Sim, C.W. Lee, T. Choi, H. Jung, Y. Kim, Z. Lee, J. Myoung, C. Dussarrat, C.L. Matras, J. Park, H. Choi, H. Kim, Controllable synthesis of molubdenum tungsten disulfide alloy for vertically composition-controlled multilayer, Nat. Comm. 6 (2015) 7817–7826.
[48] M.B. Sreedhara, S. Gope, B. Vishal, R. Datta, A.J. Bhattacharyya, C.N.R. Rao, Atomic layer deposition of crystalline epitaxial MoS_2 nanowall networks exhibiting superior performance in thin-film rechargeable Na-ion batteries, J. Mater. Chem. A. 6 (2018) 2302–2310.
[49] E. Østreng, K.B. Gandrud, Y. Hu, O. Nilsen, H. Fjellvag, High power nano-structured V_2O_5 thin film cathodes by atomic layer deposition, J. Mater. Chem. A 2 (2014) 15044–15051.
[50] D.K. Nandi, U.K. Sen, S. Sinha, A. Dhara, S. Mitra, S.K. Sarkar, Atomic layer deposited tungsten nitride thin films as a new lithium-ion battery anode, Phys. Chem. Chem. Phys. 17 (2015) 17445–17453.